OPEN ACCESS
IOP Publishing
Journal of Physics D: Applied Physics
J. Phys. D: Appl. Phys. **58** (2025) 145101 (7pp)
https://doi.org/10.1088/1361-6463/adb317

Splitting of the absorption edge in the topological insulator $Bi_{1.1}Sb_{0.9}Te_2S$: mid-infrared magneto-optical study

M V Yakushev[1,2,3,4,*], T V Kuznetsova[1], D V Belyaev[1], V I Grebennikov[1,4], M Orlita[5,6], G Martinez[5], K A Kokh[7], R W Martin[2] and O E Tereshchenko[1,8]

[1] M.N. Miheev Institute of Metal Physics Ural Branch of the Russian Academy of Sciences, Ekaterinburg 620108, Russia
[2] Department of Physics, SUPA, Strathclyde University, Rottenrow 107, G4 0NG Glasgow, United Kingdom
[3] Institute of Solid State Chemistry, Ural Branch of the Russian Academy of Sciences, 620990 Ekaterinburg, Russia
[4] Ural State University of Railway Transport, 620034 Ekaterinburg, Russia
[5] Laboratoire National des Champs Magnétiques Intenses (LNCMI), Grenoble, France
[6] Faculty of Mathematics and Physics, Charles University, Ke Karlovu 5, Prague 121 16, Czech Republic
[7] Institute of Geology and Mineralogy, Siberian Branch of the Russian Academy of Sciences, Novosibirsk 630090, Russia
[8] Institute of Semiconductor Physics, Siberian Branch of the Russian Academy of Sciences, Novosibirsk 630090, Russia

E-mail: michael.yakushev@strath.ac.uk

Received 26 October 2024, revised 13 January 2025
Accepted for publication 6 February 2025
Published 18 February 2025

Abstract

External magnetic fields can be used to control the spin properties of charge carriers in topological insulators (TIs). Thin p-type layers of the TI $Bi_{1.1}Sb_{0.9}Te_2S$ were studied using mid-infrared Fourier transform magneto-transmission spectroscopy in magnetic fields up to 11 T. Zero field spectra, measured at 4.2 K and 300 K, demonstrated a sharp absorption edge, used to determine an optical bandgap E_g^{opt} of 0.31 and 0.22 eV, respectively, as well as to establish the direct character of the bandgap. Fabry–Perot oscillations were used to estimate a refractive index of 6.4. A difference of E_g^{opt} from the bandgap, determined earlier by angular resolved photoelectron spectroscopy, was attributed to the formation of band tails generated by high concentrations of randomly distributed charged defects. Equal electron m_e and hole m_h effective masses of $0.152m_0$ were determined using a theoretical model employing simplified Dirac-type Hamiltonian. Magnetic fields split the absorption edge and the non-linear character of this splitting energy resulted in a strong decrease of the g-factor with increasing field.

Keywords: topological insulators, magneto-transmission, Lande g-factor, $Bi_{1.1}Sb_{0.9}Te_2S$

* Author to whom any correspondence should be addressed.

1. Introduction

Topological insulators (TIs), such as the model compounds Bi_2Se_3, Bi_2Te_3 and Sb_2Te_3 belong to a new class of three-dimensional materials combining an insulator like bulk with topologically protected surface states (TSSs) that can be described by Dirac cone type dispersion relations [1–4]. Prospects of the application of TIs in quantum electronics [5] and spintronics [6] attract significant attention from the research community. However, the electronic properties of the model TI materials are not quite suitable for straight forward applications which require a wider bandgap E_g and the energy position of the Dirac point at the bandgap centre. These can be achieved in solid solutions fabricated by the simultaneous incorporation of S and Sb to Bi_2Te_3 [7, 8] resulting in the quaternary compound $Bi_{1.1}Sb_{0.9}Te_2S$ which is a very promising TI for the development of spintronic devices due to its comparatively wide bandgap and the energy position of the Dirac cone near its centre [8, 9]. Despite its high potential very little so far has been reported on the electronic and optical properties of this rather novel material.

The research community studying TIs mostly concentrates on non-trivial electronic properties related to their TSS. However, their bulk also reveals interesting properties: a symmetry of the conduction and valence bands in Bi_2Se_3 [10] and Bi_2Te_3 [11] along with an extraordinary large Verdet constant due to a strong Faraday rotation effect which results in a large splitting of the absorption edge in magnetic fields due to giant g-factors [12]. Such effects have not been explored as yet for $Bi_{1.1}Sb_{0.9}Te_2S$.

Angular resolved photoelectron spectroscopy (ARPES) is amongst the most popular techniques for experimentally establishing the electronic structure in conventional solid-state materials in general and TIs in particular [1, 13–15]. However, methods of optical and magneto-optical spectroscopy can also provide accurate information on the electronic properties [16, 17], help determine such vital parameters as E_g of the bulk of TIs [18], charge carrier masses and examine the Zeeman effect [10–12] which is critical for understanding the coupling of electron spins with external magnetic fields used to control the spin properties in TIs.

In this paper the optical and electronic properties of the TI $Bi_{1.1}Sb_{0.9}Te_2S$ were examined in the region of the fundamental absorption edge using mid-infrared (MIR) Fourier transform (FT) magneto-transmission spectroscopy at magnetic fields up to 11 T.

2. Experimental details

A single crystalline ingot of $Bi_{1.1}Sb_{0.9}Te_2S$ was grown from the high purity elements Bi, Sb, Te and S using the vertical Bridgman technique [9]. Flat samples with sizes of 5×5 mm^2 and thicknesses of 3 mm were cut from the ingot along the hexagonal planes (0001). Free-standing layers with a thickness of 5 μm were exfoliated for transmission measurements and placed on copper foils over 2×2 mm^2 holes.

The structural properties of the samples, examined by x-ray diffraction and ARPES, the elemental composition, analysed by energy dispersive x-ray microanalysis as well as transport properties, measured in the (0001) plane using perpendicular magnetic fields B, have been reported previously [9].

The p-type conductivity and hole concentrations of 2.3×10^{19} and 3.5×10^{19} cm^{-3} at room temperature and 77 K, respectively, were determined earlier by Hall measurements [9].

Near normal incidence MIR range transmission and reflectivity measurements were carried out at the Laboratoire National des Champs Magnétiques Intenses (Grenoble, France) in the spectral range from 0.05 to 0.6 eV at 4.2 K using a Bruker IFS 66 v/S FT vacuum spectrometer with globar light source and silicon bolometer as a detector. Magnetic fields up to 11 T, generated by a superconducting magnet and applied in the Faraday configuration with $\boldsymbol{B}$ perpendicular to the (0001) plane, were used to carry out magneto-transmission measurements. Each transmission spectrum was normalised by that of the globar source light measured through an aperture attenuating the intensity to take in account variations in the bolometer response induced by the magnetic fields.

3. Results and discussion

Zero-field MIR transmission spectra, measured at 4.2 K and 300 K, are shown in figure 1(a) whereas a MIR reflectivity spectrum taken at 4.2 K is shown in figure 1(b). Both transmission spectra reveal a sharp fundamental absorption band edge at about 0.31 eV at 4.2 K and 0.22 eV at 300 K as well as significant Fabry–Perot (FP) oscillations showing that the top and bottom surfaces of the sample are quite parallel. The reflectivity spectrum reveals a plasma edge and two TO phonons in the far infrared region [9] whereas in the MIR region the spectrum is rather featureless.

The absorption coefficient (α) near the interband edge was calculated using the 4.2 K MIR transmission T and reflectivity R spectra shown in figures 1(a) and (b), respectively [19]:

$$\alpha = -\frac{1}{d}\ln\left[-\frac{(1-R)^2}{2TR^2} + \sqrt{\left(\frac{(1-R)^4}{4T^2R^4} + \frac{1}{R^2}\right)}\right]. \quad (1)$$

Figure 3(a) reveals a relatively sharp fundamental absorption edge. The magnitude of the absorption coefficient above the bandgap exceeds $\alpha = 8 \times 10^4$ cm^{-1} whereas at photon energies below the gap it also has a rather high value of $\alpha = 10^4$ cm^{-1}. We attribute the high absorption at sub-gap energies to a high concentration of defects with energy levels within the bandgap.

Magnetic fields had a profound effect on the shape of the absorption edge in the transmission spectra as shown in

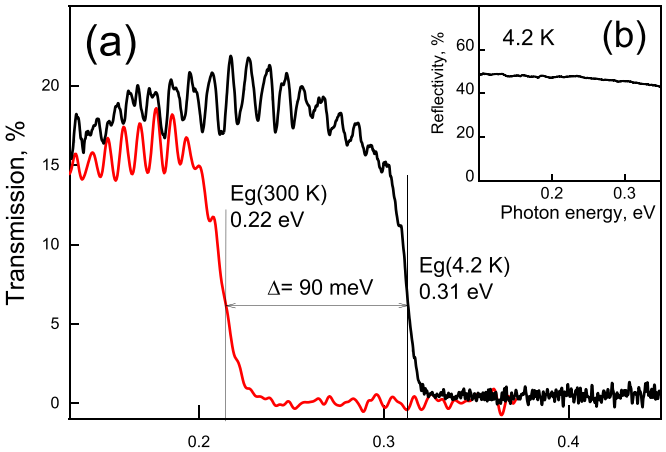

Figure 1. Zero field MIR transmission spectra measured at 300 K and 4.2 K(a), zero field 4.2 K MIR reflectivity spectrum (b).

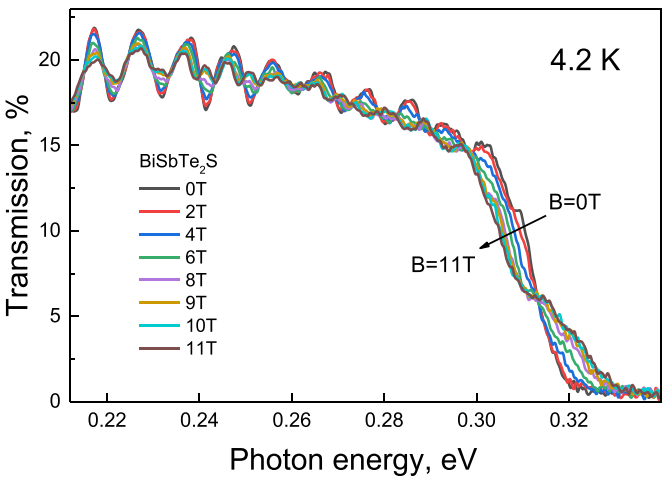

Figure 2. Effects of magnetic fields on the MIR transmission spectrum at the absorption edge.

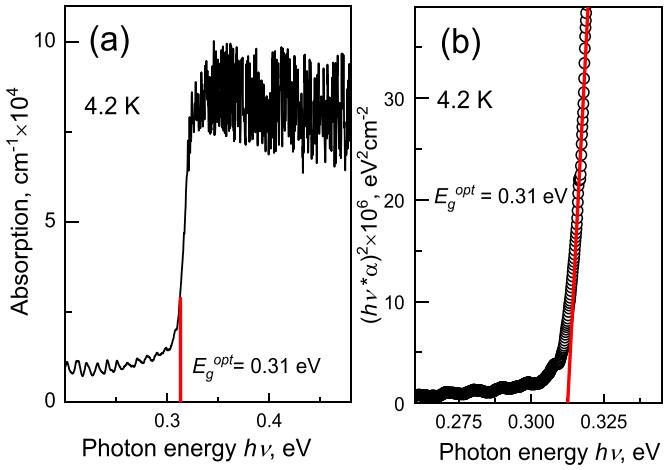

Figure 3. Absorption coefficient α at 4.2 K (a), the straight line fit to the linear part of the $(\alpha h\nu)^2$ dependence on photon energy giving E_g^{opt} (b).

figure 2. The top part of the spectrum gradually shifts towards lower energies whereas the bottom one shifts to higher ones resulting in an *S*-shaped band edge with the pivoting point at 0.31 eV. The magnetic fields also result in a significant decrease in the amplitude of the FP oscillations which can be attributed to the Faraday effect [20].

Assuming a direct character of the bandgap, demonstrated by the ARPES measurements [9], we determined an optical bandgap of $E_g^{opt} = (0.31 \pm 0.02)$ eV by extrapolating a line best fit to the linear part of the $(\alpha h\nu)^2$ dependence on the photon energy as shown in figure 3(b). The resulting E_g^{opt} coincides well with the spectral position of the pivoting point in the magneto-transmission spectra in figure 2. An optical gap of 0.22 eV, estimated from the transmission spectrum measured at 300 K, reveals a 90 meV bandgap shrinking. A similar bandgap shrinking with increasing temperature was reported for the model binary TIs Bi_2Se_3, Bi_2Te_3 as well as Sb_2Te_3 and assigned to both thermal expansion and electron–phonon coupling [21].

Unlike in *n*-type Bi_2Se_3, where E_g^{opt} exceeds E_g due to the Burstein–Moss effect [10, 18] E_g^{opt} in our p-type $Bi_{1.1}Sb_{0.9}Te_2S$ is smaller than E_g determined by ARPES (0.37 eV), suggesting a bandgap narrowing. In highly doped p-type compound semiconductors such narrowing is often associated with band tails formed by high concentrations of randomly distributed charged defects which modify the density of states at the band edge [22]. In compound semiconductors such defects, both donors and acceptors, can be formed by nanometre-scale deviations in the elemental composition from the ideal stoichiometry resulting in spatial potential fluctuations [23] as shown in figure 4. Such fluctuations, also observed in the TI Bi_2Te_2Se, were attributed to Bi/Te antisite defects [24]. Theoretical studies on other semiconductor compounds reveal that the formation of intrinsic acceptors reduces the formation energy of donors resulting in a compensation [25]. Although the conductivity of the examined sample, measured by Hall effect, is p-type this sample is likely to be compensated. The measured acceptor concentration would be the difference between the concentration of acceptors and donors [26]. Therefore, we propose that apart from high concentrations of acceptors the $Bi_{1.1}Sb_{0.9}Te_2S$ sample can also contain a high concentration of donors leading to a significant degree of compensation and the presence of band tails at both the valence as well as the conduction bands.

Assuming a symmetry of the valence and conduction bands the mean depth of the band tails γ can be estimated as $\gamma_e \approx \gamma_h \approx (E_g - E_g^{opt})/2 \approx 30$ meV.

The FP interference oscillations in the transmission spectrum, which can be seen in figure 1, were used to estimate the refractive index n of $Bi_{1.1}Sb_{0.9}Te_2S$ near the absorption edge: $n = \lambda_1\lambda_2/[(\lambda_1 - \lambda_2)2d]$, where λ_1 and λ_2 are the wavelengths of two adjacent maxima or minima in the transmission spectrum plotted with wavelength as the argument [27, 28].

The determined value of n has a weak dependence on the spectral energy, increasing from 6.0 at 0.112 eV to 7.4 at 0.313 eV. This results in an average value of $n \approx 6.4$ over the spectral range from 0.112 eV to 0.313 eV and is close to $n \approx 6$ reported for Bi_2Se_3 [12]. To evaluate modifications of the transmission spectra under magnetic fields these spectra

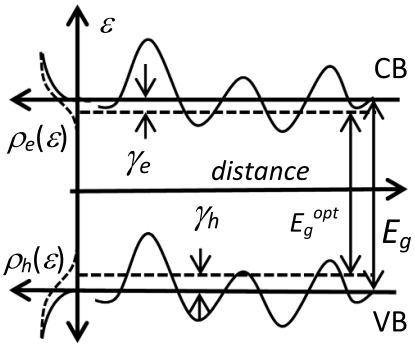

Figure 4. A schematic energy diagram illustrating the formation of band tails with average depths γ_e and γ_h for the conduction (CB) and valence (VB) band, respectively. Spatial potential fluctuations modify the density of states $\rho_c(\varepsilon)$ and $\rho_h(\varepsilon)$ for CB and VB, respectively.

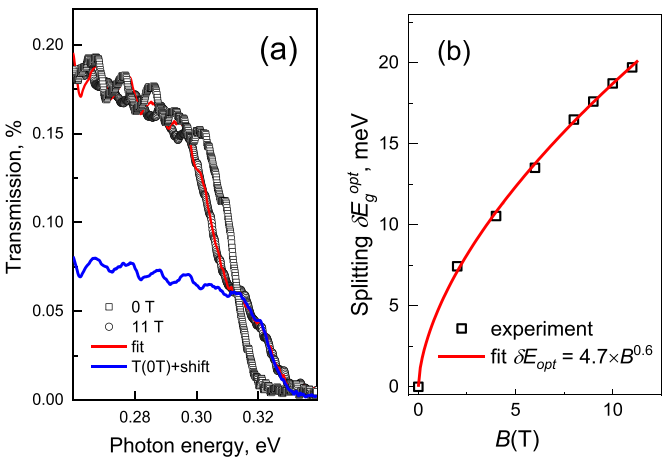

Figure 5. (a) MIR transmission spectrum at $B = 0$ T (□) and $B = 11$ T (○) fitted with the sum of two shifted and scaled zero field transmission spectra (red solid line). The attenuated zero field spectrum, shifted towards higher energies, is shown by blue solid line. (b) Dependence of the energy splitting $\delta E_g{}^{opt}$ on B, experimental values (□), fit (red solid line).

were fitted with sums of two zero field MIR transmission spectra. One of these spectra is shifted towards lower energies whereas the other is shifted towards higher energies. The intensity of the shifted spectra was attenuated to fit their sum to the experimental data. An example of such fitting is shown in figure 5(a), for $B = 11$ T.

It can be seen that the sum of two shifted zero field spectra closely matches the experimental data at the absorption edge, whereas small mismatches at energies below 0.3 eV are mostly due to differences in the amplitude and phase of the FP oscillations. The dependence of the experimentally determined values of the splitting of the two fitting spectra on the magnetic field $\delta E_g{}^{opt}(B)$ is plotted in figure 5(b).

This dependence reveals a significantly non-linear increase of $\delta E_g{}^{opt}$ at fields rising from zero to 4 T whereas at higher fields, in excess of 6 T $\delta E_g{}^{opt}(B)$ converges to a more linear dependence on B. The experimental points, fitted by the empirical function $\delta E_g{}^{opt}(B) = 4.7 \times B^{0.6}$, are shown in figure 5(b).

Table 1. Parameters of the electronic structure in $Bi_{1.1}Sb_{0.9}Te_2S$, calculated using the Dirac-type Hamiltonian model.

$E_{g\,opt}$(4.2 K)	m_D	m_e, m_h	g_e, g_h
0.31 eV	$0.076m_0$	$0.152m_0$	26

To understand the effect of splitting let us consider the electronic band structure of this material.

According to ARPES studies [9] $Bi_{1.1}Sb_{0.9}Te_2S$ is a direct bandgap semiconductor with near parabolic conduction and valence bands. Therefore, we can employ a simplified model based on the Dirac-type Hamiltonian [29, 30] proposed to describe the electronic properties of TIs [10].

According to this model two parameters, the band gap E_g and the Dirac velocity υ_D, determine the Dirac mass as $m_D = E_g/(2\upsilon_D{}^2)$. Therefore, we calculated $m_D = 0.076m_0$ (where m_0 is the free electron mass) assuming that this velocity is 6.5×10^5 ms^{-1} for $Bi_{1.1}Sb_{0.9}Te_2S$ [9].

The model proposes symmetry of the valence and conduction bands and determines the electron m_e and hole m_h effective masses as $m_e \approx m_h \approx 2m_D$. Therefore, we can find $m_e \approx m_h \approx 0.152m_0$. These masses are collected in table 1. The Dirac mass in $Bi_{1.1}Sb_{0.9}Te_2S$, is slightly smaller than $m_D = 0.08m_0$, calculated employing such a model, in Bi_2Se_3, which is also a direct bandgap semiconductor with near parabolic conduction and valence bands [10]. The electron and hole effective masses in Bi_2Se_3, derived from its Dirac mass assuming the symmetry, are in a good agreement with those determined from experiments, support the model.

Magnetic fields lift the spin degeneracy of the charge carriers in the valence and conduction bands splitting the absorption edge in the transmission spectra of $Bi_{1.1}Sb_{0.9}Te_2S$ by $\delta E_g{}^{opt}$. Figure 6 shows a simplified diagram of dispersion relations (energy versus momentum in the top part of the figure) in comparison with the splitting in the transmission spectrum at $B = 11$ T (in the bottom part of the figure) illustrating the nature of such a splitting.

Assuming the Zeeman formula and symmetry of the carrier masses $m_e = m_h$ we can calculate $\delta E_g{}^{opt}$ as:

$$\delta E_g^{opt}(B) = \mu_B B g, \tag{2}$$

where μ_B is the Bohr magneton, $g = g_e + g_h$ is the effective Lande-factor and, g_e and g_h are for the electrons and holes, respectively. The symmetry of the valence and conduction bands should result in the symmetry of the electron and hole Lande-factors: $g_e \approx g_h \approx 2m_0/m_D$. Therefore, for $Bi_{1.1}Sb_{0.9}Te_2S$ we estimate theoretical values of $g_e \approx g_h \approx 26$.

A similar splitting of the absorption edge under magnetic fields has been reported for Bi_2Se_3 [10] where values of $g_e = g_h \approx 25$, calculated using the same model. The linear dependence of $\delta E_g{}^{opt}$ on B for Bi_2Se_3 reported in [12] resulted in a constant rate of such splitting $\delta E_g{}^{opt}/B = 2.6$ meV T^{-1} for B below a saturation limit [31]. This, in turn, led to an independence of its g-factor with respect to B. However, the dependence of such a rate of splitting on B for $Bi_{1.1}Sb_{0.9}Te_2S$, shown in figure 7(a), is quite different.

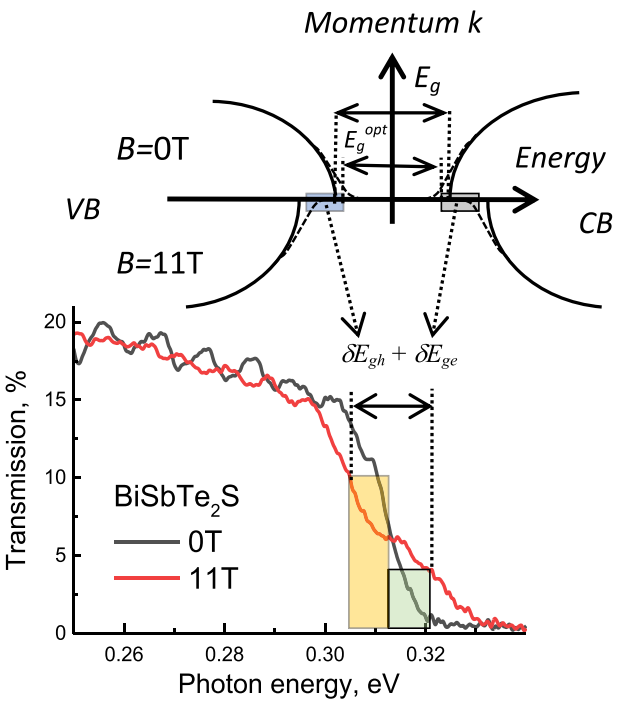

Figure 6. A schematic diagram of the effect of magnetic fields on the valence (VB) and conduction (CB) bands at the Γ point of the Brillouin zone (momentum versus energy in the upper part of the figure) in comparison with the splitting in the transmission spectrum at $B = 11$ T in the lower part of the figure.

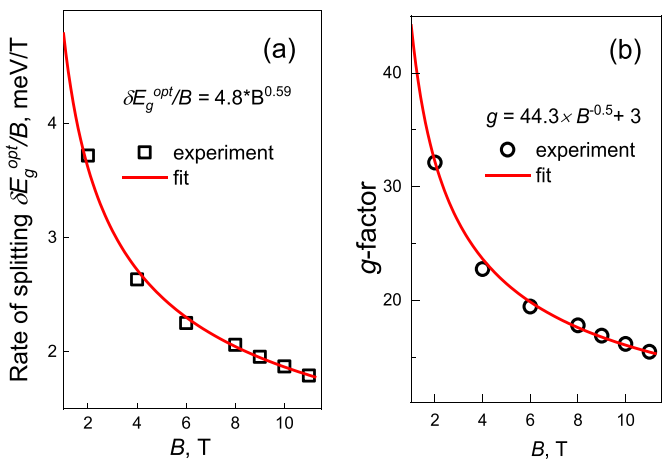

Figure 7. The dependence of the rate of splitting $\delta E_g^{opt}/B$ (a) and the g-factor (b) on the magnetic field B. Symbols are experimental points, red solid lines are fitted empirical functions diverging at $B \to 0$.

The non-linearity of δE_g^{opt} with respect to B, shown in figure 5(b), results in a dependence of its rate $\delta E_g^{opt}/B$ on B decreasing from 3.7 meV T^{-1} for $B = 2$ T to 1.8 meV T^{-1} for $B = 11$ T. Figure 7(a) also shows the empirical function $4.8 \times B^{0.59}$ fitted to the experimental data for $\delta E_g^{opt}/B$. The effective g-factor for $Bi_{1.1}Sb_{0.9}Te_2S$, determined for the experimental points using equation (2), are shown in figure 7(b). These points were fitted with the empirical function $g(B) = 4.8 \times B^{-0.5}$ which is also shown in figure 7(b). The sharp reduction of the g-factor at low magnetic fields is followed by its near saturation at 11 T to $g = 15$. A saturation of the absorption edge splitting in magneto-transmission spectra of Bi_2Se_3 with increasing B was reported earlier [31].

However, this saturation was observed for rather high magnetic fields in excess of 22 T whereas at fields below this value a linear increase of the splitting and a field independent g-factor were reported.

In the case of $Bi_{1.1}Sb_{0.9}Te_2S$ the observed saturation is quite different. The rate of shift as well as g reveal a diverging increase at $B \to 0$ whereas at higher fields one can see a gradual reduction of g leading to an almost linear dependence of g on B at fields above 6 T.

A similar diverging dependence of the g-factor on B, at $B \to 0$ observed for HgCdTe [32], was attributed to a high strength of the spin–orbital coupling so the spin splitting in this material is mostly determined by orbital parameters.

On the other hand, the influence of potential fluctuations, generated by inhomogeneously distributed charged defects in the TI Sb_2Te_2Se, on the Zeeman shift of the zeroth Landau level energy (δE_{0LL}), was taken into account by adding an additional, inversely dependent on magnetic field $1/B$ term to the dependence of δE_{0LL} on B [33].

In general, $Bi_{1.1}Sb_{0.9}Te_2S$ and Bi_2Se_3 are composed of different elements which influence the wave functions of these materials resulting in different orbital characters and different g-factors. Further studies are required to understand the origin of such a dependence of g on B in $Bi_{1.1}Sb_{0.9}Te_2S$.

4. Conclusions

About 5 μm thick layers, cleaved along the hexagonal planes (0001) from a p-type single crystal of the TI $Bi_{1.1}Sb_{0.9}Te_2S$ grown by the vertical Bridgeman technique, were studied using MIR FT magneto-transmission spectroscopy. Zero field spectra demonstrated a sharp absorption edge at 0.31 eV and significant FP oscillations which were used to estimate a mean refraction index of $n = 6.4$.

Absorption spectra demonstrated an above gap absorption coefficient of 8×10^4 cm^{-1} compared to 10^4 cm^{-1} within the bandgap, which was assigned to high concentration of defects. An optical bandgap E_g^{opt} of 0.31 eV at 4.2 K was determined from the absorption spectra assuming a direct bandgap. The significant difference of E_g^{opt} from E_g, found earlier using ARPES, was attributed to the formation of band tails due to high concentrations of charged defects. An optical bandgap of 0.22 eV was estimated from the transmission spectra measured at 300 K.

Magnetic fields, applied in the Faraday configuration, split the absorption edge in the transmission spectra. The g-factor of the splitting, determined assuming the Zeeman formula, demonstrates a dependence on B sharply decreasing from $g = 32$ at $B = 2$ T to $g = 15$ at $B = 11$ T. A non-linear character of the energy splitting with respect to B resulted in a strong decrease of the g-factor with increasing B.

Charge carrier masses $m_e \approx m_h \approx 0.152m_0$ were calculated using a theoretical model employing simplified Dirac-type Hamiltonians under the assumption of the direct character of the bandgap, symmetry and parabolicity of the valence as well as conduction bands. However, such calculations with respect to the splitting of the band edge in the transmission spectra resulted in a significant difference of the g-factors calculated using the model and those determined experimentally.

Data availability statement

All data that support the findings of this study are included within the article.

Acknowledgment

The research was carried out within the state assignment of the Ministry of Science and Higher Education of the Russian Federation ('Spin' No 122021000036-3). Crystal growth was performed under the state assignment IGM SB RAS 122041400031-2. The authors acknowledge the support of the LNCMI-CNRS in Grenoble as a member of the European Magnetic Field Laboratory (EMFL). The UK authors are grateful for the travel expenses reimbursement: projects EP/X020304/1 and NS/A000060/1.

ORCID iDs

M V Yakushev https://orcid.org/0000-0002-1375-1239
T V Kuznetsova https://orcid.org/0000-0003-4302-9607
V I Grebennikov https://orcid.org/0000-0003-1099-307X
M Orlita https://orcid.org/0000-0002-9633-507X
G Martinez https://orcid.org/0000-0001-6277-6769
K A Kokh https://orcid.org/0000-0003-1967-9642
R W Martin https://orcid.org/0000-0002-6119-764X
O E Tereshchenko https://orcid.org/0000-0002-1375-1239

References

[1] Hasan M Z and Kane C L 2010 Colloquium: topological insulators *Rev. Mod. Phys.* **82** 3045–67
[2] Ando Y 2013 Topological insulator materials *J. Phys. Soc. Japan* **82** 102001
[3] Sheregii E M, Cebulski J, Marcelli A and Piccinini M 2009 Temperature dependence discontinuity of the phonon mode frequencies caused by a zero-gap state in hgcdte alloys *Phys. Rev. Lett.* **102** 045504
[4] Woźny M, Szuszkiewicz W, Dyksik M, Motyka M, Szczerbakow A, Bardyszewski W, Story T and Cebulski J 2024 Electron–phonon coupling and a resonant-like optical observation of a band inversion in topological crystal insulator $Pb_{1-}xSn_xSe$ *New J. Phys.* **26** 063008
[5] Fu L and Kane C L 2008 Superconducting proximity effect and majorana fermions at the surface of a topological insulator *Phys. Rev. Lett.* **100** 096407
[6] Moore J E 2010 The birth of topological insulators *Nature* **464** 194–8
[7] Annese E *et al* 2018 Electronic and spin structure of the wide-band-gap topological insulator: nearly stoichiometric Bi_2Te_2S *Phys. Rev.* B **97** 205113
[8] Ji H, Allred J M, Fuccillo M K, Charles M E, Neupane M, Wray L A, Hasan M Z and Cava R J 2012 $Bi_2Te_{1.6}S_{1.4}$: a topological insulator in the tetradymite family *Phys. Rev.* B **85** 201103
[9] Khatchenko Yu E *et al* 2022 Structural, optical and electronic properties of the wide bandgap topological insulator $Bi_{1.1}Sb_{0.9}Te_2S$ *J. Alloys Compd.* **890** 161824
[10] Orlita M *et al* 2015 Magneto-optics of massive dirac fermions in bulk Bi_2Se_3 *Phys. Rev. Lett.* **114** 186401
[11] Mohelský I *et al* 2020 Landau level spectroscopy of Bi_2Te_3 *Phys. Rev.* B **102** 085201
[12] Ohnoutek L *et al* 2016 Strong interband Faraday rotation in 3D topological insulator Bi_2Se_3 *Sci. Rep.* **6** 19087
[13] Chen Y L *et al* 2009 Experimental realization of a three-dimensional topological insulator, Bi_2Te_3 *Science* **325** 178–81
[14] Ortmann F, Roche S, Valenzuela S O and Molenkamp L W 2015 *Topological Insulators: Fundamentals and Perspectives* (Wiley)
[15] Locatelli L, Kumar A, Tsipas P, Dimoulas A, Longo E and Mantovan R 2022 Magnetotransport and ARPES studies of the topological insulators Sb_2Te_3 and Bi_2Te_3 grown by MOCVD on large-area Si substrates *Sci. Rep.* **12** 3891
[16] Chapler B C, Post K W, Richardella A R, Lee J S, Tao J, Samarth N and Basov D N 2014 Infrared electrodynamics and ferromagnetism in the topological semiconductorsBi_2Te_3 and Mn-doped Bi_2Te_3 *Phys. Rev.* B **89** 23
[17] Sushkov A B, Jenkins G S, Schmadel D C, Butch N P, Paglione J and Drew H D 2010 Far-infrared cyclotron resonance and Faraday effect in Bi_2Se_3 *Phys. Rev.* B **82** 12
[18] Martinez G *et al* 2017 Determination of the energy band gap of Bi_2Se_3 *Sci. Rep.* **7** 6891
[19] Allaham M, Dallaev R, Burda D, Sobola D, Nebojsa A, Knápek A, Mousa M S and Kolařík V 2024 Energy gap measurements based on enhanced absorption coefficient calculation from transmittance and reflectance raw data *Phys. Scr.* **99** 025952
[20] Kovalenko Yu E, Yakushev M V, Grebennikov V I, Orlita M, Titova S G, Kokh K A, Tereshchenko O E and Kuznetsova T V 2024 Electronic properties of the topological insulator Sb_2Te_2Se *Semiconductors* **58** 185–8
[21] Monserrat B and Vanderbilt D 2016 Temperature effects in the band structure of topological insulators *Phys. Rev. Lett.* **117** 226801
[22] Kane E O 1963 Perturbation-moment method: application to band structure of impure semiconductors *Phys. Rev.* **131** 1532–42
[23] Shklovskii B I and Efros A L 1984 *Electronic Properties of Doped Semiconductors* (Springer)
[24] Fu Y-S, Hanaguri T, Yamamoto S, Igarashi K, Takagi H and Sasagawa T 2013 Memory effect in a topological surface state of Bi_2Te_2Se *ACS Nano* **7** 4105–10
[25] Zhang S B, Wei S-H, Zunger A and Katayama-Yoshida H 1998 Defect physics of the $CuInSe_2$ chalcopyrite semiconductor *Phys. Rev.* B **57** 9642–56
[26] Rau U and Schock H W 1999 Electronic properties of Cu(In,Ga)Se_2 heterojunction solar cells–recent achievements, current understanding, and future challenges *Appl. Phys.* A **69** 131–47
[27] Swanepoel R 1983 Determination of the thickness and optical constants of amorphous silicon *J. Phys. E: Sci. Instrum.* **16** 1214–22
[28] Pankove J I 1971 *Optical Processes in Semiconductors* (NJ Prentice-Hall)

[29] Aguilera I, Friedrich C, Bihlmayer G and Blügel S 2013 *G W* study of topological insulators Bi_2Se_3, Bi_2Te_3, and Sb_2Te_3: beyond the perturbative one-shot approach *Phys. Rev.* B **88** 045206
[30] Zhang H, Liu C-X, Qi X-L, Dai X, Fang Z and Zhang S-C 2009 Topological insulators in Bi_2Se_3, Bi_2Te_3 and Sb_2Te_3 with a single Dirac cone on the surface *Nat. Phys.* **5** 438–42
[31] Hakl M *et al* 2017 The saturation of interband Faraday rotation in Bi_2Se_3 *EPL* **117** 47006
[32] Orlita M *et al* 2014 *Nat. Phys.* **10** 233–8
[33] Fu Y-S, Hanaguri T, Igarashi K, Kawamura M, Bahramy M S and Sasagawa T 2016 Observation of Zeeman effect in topological surface state with distinct material dependence *Nat. Commun.* **7** 10829